Experimental Testing and Modeling of Seismically Rehabilitated RC Bridge Piers Using Shape Memory Alloys

M. Shin and B. Andrawes
Department of Civil and Environmental Engineering, University of Illinois at Urbana-Champaign, USA

15 WCEE
LISBOA 2012

SUMMARY:
This study focuses on examining experimentally a novel concept for seismic retrofitting and emergency repair of reinforced concrete (RC) bridge piers. It investigates the feasibility of using shape memory alloy (SMA) spirals to: 1) enhance the flexural ductility of vulnerable RC piers and mitigate their level of damage under strong seismic event, and 2) conduct emergency repair to restore the ductility and strength of severely damaged RC piers. First, four 1/3-scale RC piers with three different types of retrofitting techniques are prepared and tested under quasi-static lateral cyclic loading. Second, two severely damaged piers during the first round of testing are repaired using SMA spirals and retested. The retrofitted piers testing and the repair testing show that using SMA spirals successfully improves the performance of the RC piers and mitigate damage of the piers. An analytical model for RC bridge piers retrofitted with SMA spirals also is developed and validated.

Keywords: Active confinement, Shape memory alloys, Reinforced concrete, Modelling

1. INTRODUCTION

During historical earthquakes, numerous reinforced concrete (RC) bridges have experienced devastating failures. With the aims of preventing such failures and identifying main causes, many researches have been conducted. One of the main causes of the failures was due to the lack of flexural ductility and/or insufficient shear capacity of RC bridge piers (Chai et al. 1991; Priestley et al. 1994; Task Group 7.4 2007). The problem of lack of ductility of the RC piers can be solved by providing extra confinement externally. The external confining pressure on RC piers is traditionally applied using fiber reinforced polymer (FRP) jackets or steel jackets, and this technique is called passive confinement technique, since the confining pressure depends on the dilation of concrete under axial loading. On the other hand, the external confining pressure on the RC piers can also be applied without depending on the dilation of concrete, and this technique is often known as active confinement technique, since the confining pressure is applied prior to concrete loading. Research had demonstrated that using active confinement technique exhibits superior performance to using passive confinement technique (Richart et al. 1928); however, applying active confinement technique by prestressing conventional materials is associated with several practical complications including the need for excessive labor. Hence, this study explores the feasibility of using thermally prestressed SMA spirals for applying external active confinement pressure on RC piers. External active confinement pressure is applied to the plastic hinge zone of RC piers by heating prestrained SMA spirals which are wrapped around the piers. The active confinement pressure is associated with the large recovery stress of SMAs which is induced as a result of the SMA's attempt to recover its original shape. In this study, martensitic NiTiNb SMA wires which were prestrained to about 6%-strain by manufacturer was utilized as spirals. First, experimental testing is presented in this paper to examine of the cyclic behavior of: 1) retrofitted RC piers, and 2) repaired RC piers. Second, the experimental results are used to develop and validate analytical model for RC bridge piers retrofitted with SMA spirals.

2. RETROFIT OF RC BRIDGE PIERS

2.1 Pier Specimens and Retrofitting Techniques

Four 1/3 scale RC piers were casted and tested under quasi-static cyclic lateral loading. Fig. 2.1 shows the cross section and an isometric view of the tested piers. The lateral load was applied at the effective height of 1270 mm for each pier through a 445 kN hydraulic actuator. The diameter of the circular cross section of the piers was 254 mm, and the cover concrete was 25.4 mm. The footing of the piers was casted with the size of 1168 mm x 1168 mm x 406 mm. A constant axial load of 116 kN was applied to the top of the piers which represents 5% of the compression strength of the pier. Eight #4 steel bars were located evenly in the longitudinal direction and #2 (6 mm diameter) hoops were located laterally at 102mm. The average compressive strength of the concrete at the time of testing was found to be 44.8 MPa. Four Linear Variable Differential Transformers (LVDTs) were installed to capture the net displacement of the RC piers.

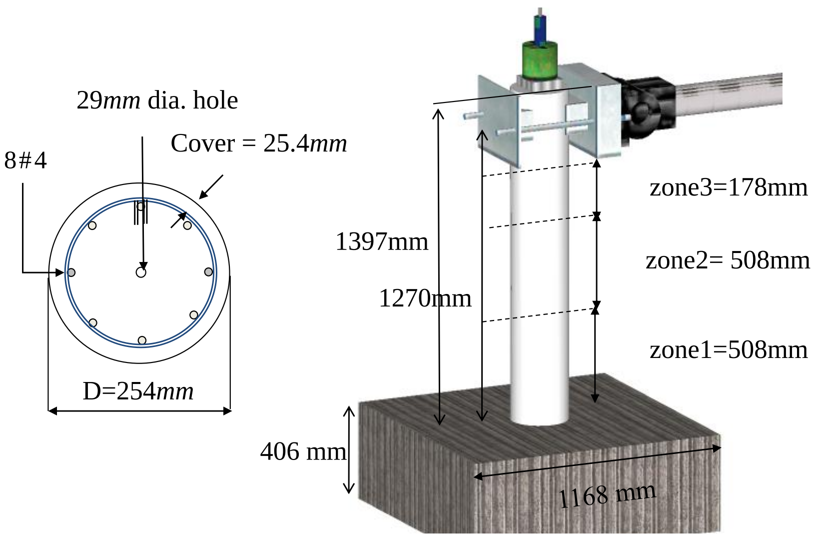

Figure 2.1. Schematic of the RC piers used in the tests

Three confining techniques were used to retrofit each pier. One pier was retrofitted with only using GFRP wraps, another was retrofitted with the SMA spirals at zone 1 (i.e. plastic hinge zone), and the other was wrapped by using GFRP jackets together with SMA spirals at zone 1. Fig. 2.2 shows each confinement applied to each pier before testing. The details of each confinement technique were summarized in Table 2.1. As indicated by the table, zone 1 was retrofitted differently in the three piers, since zone 1 was the expected plastic hinge zone. And zones 2 and 3 were retrofitted with the same GFRP jackets in all three piers. For the GFRP retrofitted pier, zone1 was wrapped with 10 layers of GFRP. For the SMA pier, 2.0 mm diameter SMA spirals were utilized to apply the same pressure produced by 10 layers of GFRP sheets at zone 1, while for the Hybrid pier, 5 layers of GFRP sheets and 20 mm pitch spacing SMA spirals were used together at zone 1, where the 20 mm pitch spacing was selected to compensate the difference of confining pressure when using 5 layers of GFRP sheets instead of 10 layers. All three retrofitted piers were designed to have the same level of confining pressure. Based on the mechanical properties of the used GFRP sheets and using an efficiency factor of 0.5 (Lorenzis and Tepfers 2003) for the GFRP jackets, the confining pressure corresponding to 10 layers of GFRP sheets was founded to be 1.5 MPa. For the SMA pier, it was found that a pitch spacing of approximately 10 mm would produce the same confining pressure of 1.5MPa based on a recovery stress of 439 MPa and a prestrain loss of 1.1%, which was determined in a separate study (Shin and Andrawes, 2010). Accordingly, using half of the GFRP sheets and SMA combined on the hybrid pier would produce the same 1.5 MPa confining pressure.

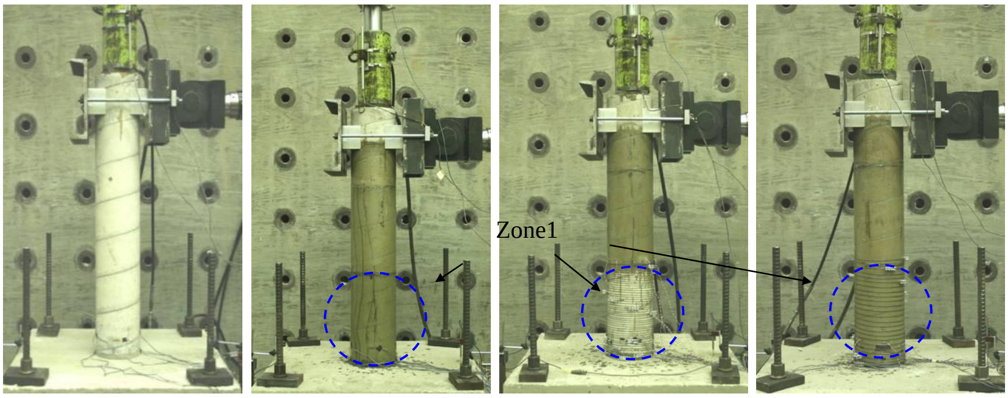

(a) As-built Pier (b) GFRP Pier (c) SMA Pier (d) Hybrid Pier

Figure 2.2. Tested Piers before testing

Table 2.1. Confinement properties of the four tested piers

	Zone1	Zone2	Zone3
As-built Pier	N/A	N/A	N/A
GFRP Pier	10 layers of GFRPs	5 layers of GFRPs	2 layers of GFRPs
SMA Pier	10mm pitch spacing SMA spirals	5 layers of GFRPs	2 layers of GFRPs
Hybrid Pier	20mm pitch spacing SMA spirals + 5 layers of GFRPs	5 layers of GFRPs	2 layers of GFRPs
Confining Pressure	1.5 MPa	0.75 MPa	0.3 MPa

2.2 Loading Protocol and Test results

The loading protocol used in the retrofit test was shown in Fig.2.3. The piers were loaded cyclically with a rate of 5.1 mm/min up to 1.5% drift ratio and 15.3 mm/min thereafter. Initially a load increment of 0.5% drift ratio was adopted until a drift ratio of 6% was reached, after which an increment of 1% was used up until 12% drift. After reaching a drift ratio of 12%, an increment of 2% was utilized.

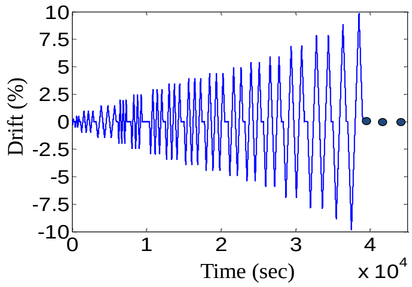

Figure 2.3. Loading protocol used in the study

The lateral force and displacement relationship of the four piers were shown in Fig. 2.4 after the test was complete. As-built pier yielded at 1.5% drift ratio and the maximum strength of the pier was found to be 34.5 kN at 2.8% drift ratio. For the GFRP retrofitted pier, the maximum strength of 35.1 kN was recorded at a drift ratio of 3.5%, and the strength of pier was gradually degraded. Finally, the recorded strength was 34.6% of the maximum strength at the final drift ratio (8%). The SMA pier showed the strength hardening until it failed, and it had the maximum strength of 36.8 kN at 12% drift ratio. The maximum strength of the Hybrid pier was found to be 37.1 kN at the 8.0% drift ratio. Also, strength hardening behavior was observed as well, which could be attributed to the elastic behavior of the SMA spirals. The failure mechanism of both the SMA pier and the Hybrid pier was due to the rupture of longitudinal reinforcement. The longitudinal reinforcement of the SMA and hybrid piers ruptured at 12% drift and 10% drift, respectively.

In order to compare the flexural ductility of each pier, the ductility ratio (μ) was calculated and shown in Fig. 2.4. The ductility ratio is defined as the ratio between the drifts at the ultimate point (measured at 80% of the ultimate strength or where longitudinal reinforcement ruptured) and the yielding point. Based on this definition, the ductility ratios of the as-built, GFRP wrapped, SMA wrapped, and SMA plus GFRP wrapped piers were 2.8, 3.3, 8.0, and 6.7, respectively. The ductility of the SMA pier and the Hybrid pier was 2.4 times and 2.0 times that of the GFRP retrofitted pier. Fig.2.4 clearly shows that the piers with the SMA spirals were able to sustain larger force and drift and dissipate significantly more hysteretic energy compared to that of the GFRP wrapped pier.

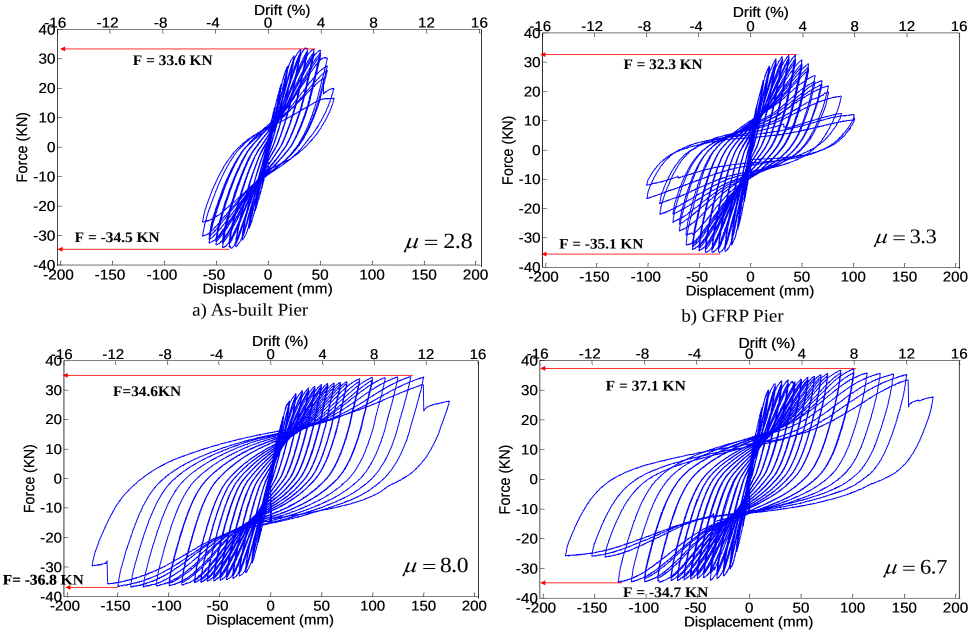

a) As-built Pier b) GFRP Pier c) SMA Pier d) Hybrid Pier

Figure 2.4. Lateral force versus drift relationships of the four tested piers

In order to understand the level of damage of each pier, Fig. 2.5 is presented. Fig. 2.5 shows the four piers after removing the wrappings and cleaning up the crushed concrete. As indicated earlier, the final drift ratios sustained by the piers were 5%, 8%, 14% and 14% for the as-built, GFRP, SMA and Hybrid pier, respectively. The widths of the remaining core concrete of the as-built, GFRP, SMA and Hybrid piers were 102mm, 102mm, 216mm, and 191mm, respectively. The piers retrofitted with SMA spirals showed the least damage among the four piers although they experienced 2.8 times and 1.75 times the maximum drift ratios of the as-built and GFRP piers, respectively. This clearly demonstrated that using SMA spirals is not only effective in improving the flexural ductility of the piers, but also in limiting their damage during earthquakes, which will have a significant impact on maintaining the post-earthquake bridge functionality.


a) As-built Pier b) GFRP Pier c) SMA Pier d) Hybrid Pier

Figure 2.5. Damaged piers after testing

3. EMERGENCY REPAIR OF SEVERELY DAMAGED PIERS

After an earthquake event, there is a dire need for an effective repair technique that could be implemented in the field in timely manner. The experimental investigation of the new confinement technique using SMA spirals was further expanded to include “emergency” repair application. Two severely damaged RC piers (the as-built pier (P1) from the retrofit testing and another pier (P2) which was accidentally damaged during testing) were repaired and retested.

3.1 Summary of Damaged Piers

3.1.1 Damage of As-built Pier P1

When the pier P1 reached the drift ratio of 3.5%, cover concrete had spalled significantly, after which, the core concrete and the two longitudinal bars located near the extreme fibers started crushing and buckling, respectively. When the pier reached 4.2% drift ratio, one of its longitudinal reinforcement ruptured, which resulted in the degradation of the strength abruptly by 23%. The maximum drift the pier experienced was 5% drift ratio. Fig. 3.1.a shows a picture of the damaged P1. The damage of the pier consisted of: 1) crushed cover and core concrete on both sides of the pier, 2) one ruptured and five buckled longitudinal reinforcement, and 3) excessive opening of transverse reinforcement.

(a) P1 (b) P2

Figure 3.1. Damage sustained by piers P1 (a) and P2 (b).

3.1.2. Damage of As-built Pier P2

A cyclic test under the same loading protocol used for the pier P1 was planned for the pier P2. However, at a drift ratio of 1.5%, the hydraulic actuator went out of control exerting a maximum drift ratio of about 7% on the specimen in one direction. Due to the accident encountered during testing, no data was recorded after the 1.5% drift. Fig. 3.1.b shows a picture of the damaged specimen under the excessive monotonic loading. Since the pier failed primarily under the monotonic loading in one direction, the concrete at one side was completely crushed, while at the other side, the concrete was cracked due to excessive tension. Therefore the damage of the pier P2 was unsymmetrical while the damage of the pier P1 was symmetrical. In addition, since the pier P2 was not subjected to significant cyclic loading at high drift ratios as the pier P1, the reinforcement of the pier P2 had buckled without experiencing any ruptures.

3.2 Repair Process

The two damaged piers were repaired by following a five-step repair process with the aim of restoring the functionalities of the piers within 24 hours. Fig. 3.2 shows each step of the repair process. First, crushed and loose pieces of concrete were removed from the damaged region of the piers. Fig. 3.2.a shows the concrete surface of the pier P1 after removing the crushed concrete. Second, slightly buckled longitudinal reinforcing bars were straightened, and the ruptured bars were connected using rebar couplers (Fig. 3.2.b). As noted earlier, only one reinforcing bar was ruptured and needed coupling in the pier P1. For the pier P2, however, no longitudinal reinforcement was ruptured, but three of the reinforcing bars severely buckled after being damaged by the excessive monotonic loading. To adjust these severely buckled reinforcing bars, it was required to cut the bars, and reconnect them with couplers. Third, pressurized epoxy was injected to fill the cracks of the concrete (Fig. 3.2.c.). From the step one though the step three, it took about three hours. Forth, quick-setting mortar was applied to the damaged region (Fig. 3.2.d). The nominal strength of the mortar at the 24 hours was recorded as 21 MPa, which is 53% of the compressive strength of the concrete used in casting the as-built piers. While curing the mortar, the fifth step of the repair process proceeded. The piers were wrapped with the SMA spirals at the repaired region (i.e. 330 mm from the pier base) with 25mm pitch spacing, and heated using a fire torch as shown in Fig. 3.2.e. Fig. 3.2.f shows a picture of the repaired pier after the completion of the repair process. It took approximately 24 hours from the first step of repair process until the onset of the pier testing. However, it is important to note that the whole repair process from the first step to the fifth step was completed in less than 15 hours.

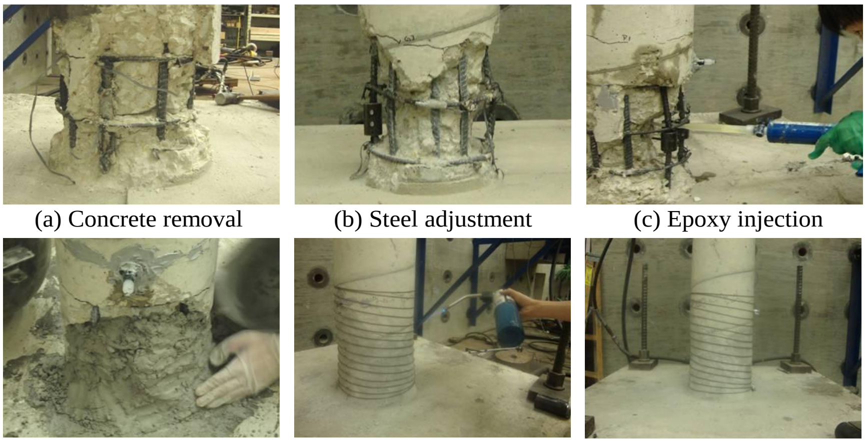

(a) Concrete removal (b) Steel adjustment (c) Epoxy injection

(d) Mortar application (e) Heating SMA spirals (f) Repaired column

Figure 3.2. Five-step emergency repair process

3.3 Emergency Repair Test Results

The lateral force and displacement relationships between the as-built and the repaired pier P1 were compared in Fig.3.3.a. The repaired pier started yielding at a drift ratio of 0.7%, and the average maximum strength recorded was 34.2 kN. At a drift ratio of 2%, the strength of the repaired pier dropped abruptly by 28% due to the rupture of one of the longitudinal reinforcement. Also another reinforcing bar was ruptured in the following cycle, and it resulted in the reduction of the strength by 48% of its maximum strength. Based on the comparison between the average strengths of the repaired and as-built piers, it was concluded that the emergency repair technique using SMA spirals performed on the severely damaged pier was capable to fully restore the as-built pier's lateral strength. Furthermore, the average initial stiffness of the repaired pier was found to be 3.4 kN/mm, which was 54% higher than that of the as-built pier and 930% higher than the residual (secant) stiffness of the damaged pier.

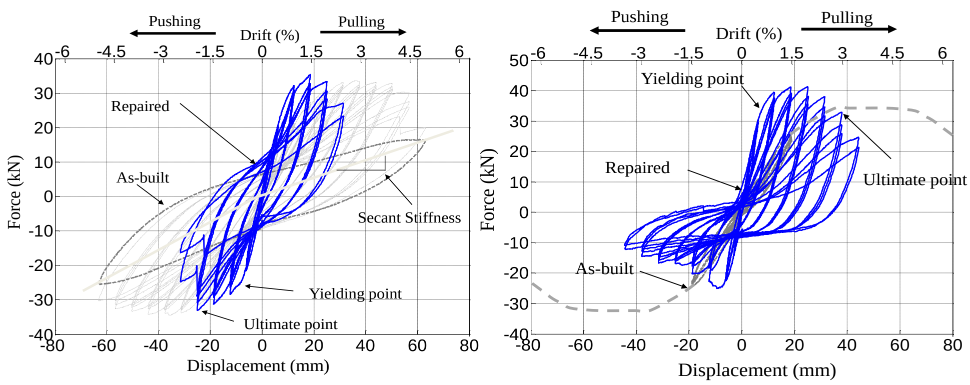

(a) P1 (b) P2

Figure 3.3. Comparison between lateral force vs. displacement relationships of the as-built (dashed line) and the repaired (solid line) pier: P1 (a) and P2 (b)

Fig.3.3.b shows the lateral force and displacement relationship between the as-built and the repaired pier P2. The repaired pier started yielding at a drift ratio of 0.6%, and the maximum strength recorded was 41.3 kN at 1.5% drift ratio. The cyclic behavior of the repaired pier P2 was unsymmetrical, and the lateral strength of the pier degraded gradually unlike the repaired pier P1 whose strength abruptly dropped. A main reason for the unsymmetrical behavior of the repaired pier P2 was due to the slippage of the coupled reinforcing bars located at one side of the repaired pier during testing. And this slippage of the reinforcing bars from the couplers caused significantly less strength of the repaired pier when it was "Pushed" (see Fig.3.3.b). On the other hand, when the pier was "Pulled", it showed satisfactory behavior since the reinforcing bars resisting tension were relatively in fair condition and only sustained minimal damage during the first round of testing. In the pulling side, the strength of the repaired pier exceeded that of the as-built pier by 21% (based on the predicted maximum strength of the as-built pier, 34.5 kN; The dashed line of the as-built pier was anticipated behaviour based on the as-built pier P1 since it were identical to the as-built P2). Also, the average initial stiffness of the repaired pier was 4.2 kN/mm, which exceeded the initial stiffness of the as-built pier by 47%.

4. MODELING OF RC BRIDGE PIER RETROFITTED WITH SMA SPIRALS

This section focuses on developing a pier model capable of describing the behavior of RC piers retrofitted with SMA spirals. OpenSees (Mazzoni et al. 2009) was utilized to model the pier and conduct a nonlinear analysis as a finite element program. Fig. 4.1 shows the schematics of a fiber section and the pier model used in the analysis. Nonlinear displacement-based beam-column element (element E2-E9) was utilized to develop the pier model with a rigid element for modeling the footing (element E1). And a rotational spring was introduced at the mid height of the footing to capture the pier's flexibility at the base. A fiber section was assigned to the beam-column elements to describe inelastic behaviors of materials; and different constitutive relationships are assigned to the fiber section for the cover concrete, core concrete, and longitudinal steel reinforcement fibers (see Fig. 4.1.a).

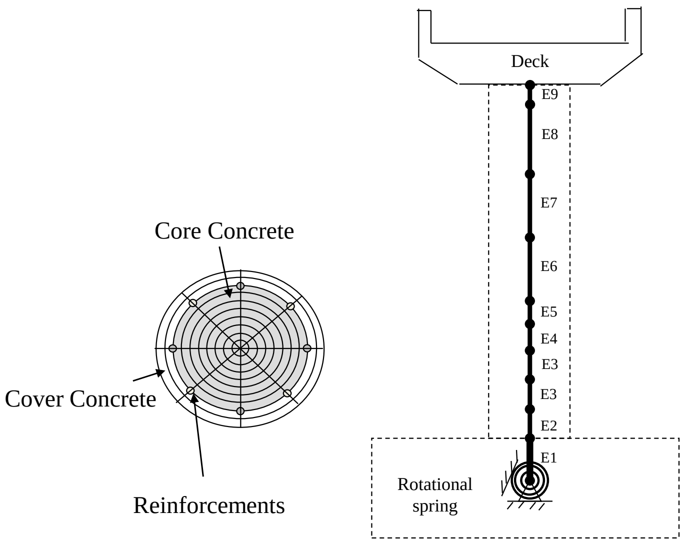

Figure 4.1. Schematics of fiber section of the pier model (a) and pier model (b)

4.1 Material Constitutive Behaviors

4.1.1 Actively Confined Concrete

The uniaxial Concrete04 material model in OpenSees was used to simulate the behavior of the concrete confined with SMA. To incorporate the effects of active confining pressure induced by the external SMA spirals, an analytical confined concrete model developed by Mander et al. (1988) was modified. In their model, Mander et al. assumed a constant confinement pressure resulting from the yielding of the steel transverse reinforcement. Furthermore, they calibrated their model using the test data obtained from multi-axial concrete cylinders subjected to active confining pressure (Schickert and Winkler 1977). According to Mander et al., the stress (f_{cc}) and strain (ε_{cc}) at the peak point of the confined concrete could be computed using Eqn. 4.1 and 4.2, respectively.

$$f_{cc} = f_{co}\left(-1.254 + 2.254\sqrt{1+\frac{7.94 f_l}{f_{co}}} - 2\frac{f_l}{f_{co}}\right), \tag{4.1}$$

$$\varepsilon_{cc} = \varepsilon_{co}\left[1+5\left(\frac{f_{cc}}{f_{co}}-1\right)\right] \tag{4.2}$$

where f_{co} and ε_{co} are the peak strength and strain of the unconfined concrete, respectively, and f_l is the effective lateral confining pressure. Since f_l inherently had an active confining feature although the equation was developed for passively confined concrete using steel reinforcement, f_l, lateral confining pressure including the confining pressure from SMA spirals was expressed as followings:

$$f_l = f_{l\_tie} + f_{l\_SMA\_active} + f_{l\_SMA\_passive} \tag{4.3}$$

where f_{l_tie} is the confining pressure induced by the internal steel ties at yielding, $f_{l\_SMA_{active}}$ is the active confining pressure from the SMA spiral, and $f_{l\_SMA\_passive}$ is the additional passive confining pressure from the SMA spiral. Once the actively confined concrete starts dilating under axial load, the pier is expected to sustain additional passive confinement pressure induced by the SMA spiral. For circular piers, the total confining pressure from SMA spirals, f_{l_SMA}, is directly related to the properties of the SMA wire through the following formula:

$$f_{l\_SMA} = k_e(2A_{SMA}(\sigma_{SMA} + \sigma_{passive}))/(d \times s) \tag{4.4}$$

where k_e is a correction factor suggested by Mander et al. to account for the reduction in the confining pressure due to the geometry of a confinement, A_{SMA} is the cross sectional area of the SMA spiral, σ_{SMA} is the SMAs recovery stress, $\sigma_{passive}$ is the additional stress induced in the SMAs due to the dilation of concrete, d is the diameter of the circular pier, s is the spiral pitch. The energy balance approach presented in Eqn. 4.5, which was also suggested by Mander et al. was adopted to calculate the ultimate strain of the confined concrete with SMA spirals.

$$U_{SMA} + U_{sh} = U_{con} + U_{sc} \tag{4.5}$$

In Eqn. 4.5, U_{SMA}, U_{sh}, U_{con}, and U_{sc} are the ultimate strain energy capacity per unit volume of core concrete for SMA spiral, transverse reinforcement, core concrete and longitudinal reinforcement, respectively. In the application of the lateral pressure, f_{l_SMA}, the spacing of the SMA spirals is considered as a key variable in controlling the confinement pressure according to Eqn. 4.4. Based on a previous experimental study by the authors, the recovery stress of SMAs was taken as 440 MPa after taking into account prestrain losses of 1% and additional stress due to the elastic behavior of SMAs under concrete dilation was taken to be 102 MPa (Shin and Andrawes 2010).

4.1.2 Longitudinal Reinforcement

The uniaxial Steel02 model in OpenSees was used to represent the nonlinear behavior of the longitudinal steel reinforcement in the SMA wrapped pier. Steel02 material model is built based upon the Giuffré-Menegotto-Pinto model (1973), and it is capable of simulating the hysteretic behavior of steel reinforcement under cyclic loading. In order to mimic the rupture of one or more of the longitudinal rebars, the rupture option of reinforcement was incorporated in the numerical simulation using the “MinMax” uniaxial material command with Steel02 material in OpenSees. When a predefined value of strain is reached, the program eliminates the stress and modulus of elasticity of Steel02 material. For longitudinal reinforcement used for the SMA pier model, an ultimate strain of 0.17 was assigned to the steel bars. This value was based on the calibration of the numerical model with the experimental data.

4.2 Model Results and Validation

The SMA pier model was subjected to the same lateral cyclic loading protocol that was used in the retrofit test. Fig. 4.2.a shows the comparison of the force-displacement relationships between the experimental result and the numerical simulation of the SMA retrofitted pier. In general, there is a good agreement between them. The pier model was able to capture the hysteretic behaviors including the rupture of the longitudinal rebar which resulted in the sudden drop in the pier strength at a drift ratio of 12%. A minor difference between the strengths of the experimental and numerical piers was observed on the pulling side. This difference was attributed to the unsymmetrical response of the experimental pier due to the accidental application of the axial load during testing with an eccentricity of approximately 15 mm.

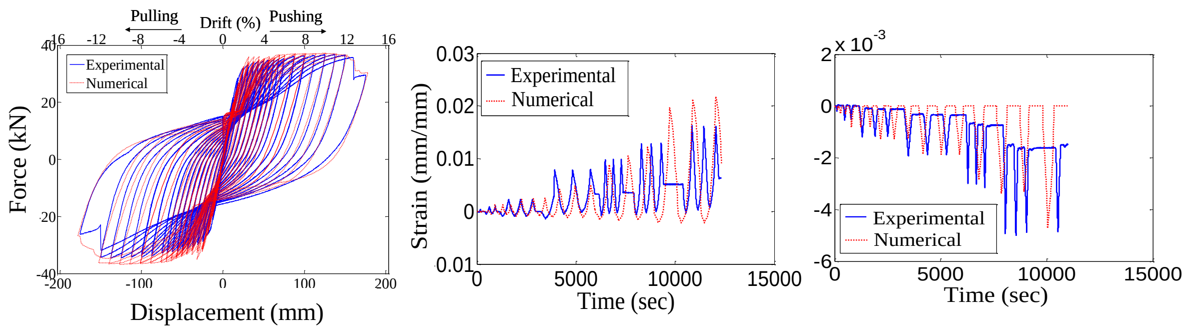

(a) Force vs. Displacement (b) Steel at the west side (c) Concrete at the west side

Figure 4.2. Comparisons between the experimental and numerical results of the force-displacement relationship (a), strains of reinforcement (b) and strains of concrete (c) of the SMA pier

Moreover, a detailed validation was performed by comparing the physical damage states observed during testing and the numerical strain-based damage states obtained from the pier model. In order to assess the damage states of the numerical model, the stress-strain behaviors of cover and core concretes and longitudinal reinforcement of the fiber section at the plastic hinge were thoroughly investigated at various locations. Damage of the pier model was defined when the concrete and steel strains reached their ultimate strain levels, and the pier model was capable of capturing the physical damage states of the tested pier including concrete cover spalling, longitudinal steel yielding, and concrete core crushing with respect to the drift level of the pier. It is worth noting that the damage of the SMA pier was not severe until the longitudinal reinforcing bars located near the extreme fibers were ruptured at 12% drift ratio. Similarly, the simulation showed that the reinforcing bar was ruptured at 12%-drift ratio when the ultimate strain of steel reached 0.17. Comparisons between the experimental and numerical strain values of longitudinal reinforcement and concrete also are presented in Fig. 4.2.b and c. The strain data were available until certain level of drift ratio since the strain gauges were damaged severely while cyclic loading progressed. Experimental data indicated that residual strains had been accumulated in the strain gauges as the testing progressed. However, the numerical strain values were not capable of exhibiting any residual strain by nature. Therefore, when taking into account the effect of the residual strains on strain gauges in each loading cycle, the experimental strain values showed better agreement with the numerical values. For instance, at a 2.5% drift ratio for concrete, the experimental compressive strain was recorded as -0.0034 mm/mm after subtracting the residual strain from the maximum compressive strain, and the numerical strain was -0.0033 mm/mm. Also, at a 2.0% drift ratio, the numerical compressive strain (-0.002 mm/mm) was 91% of the experimental strain (-0.0022 mm/mm).

5. CONCLUSIONS

This study focused on examining the feasibility of an innovative retrofit technique using SMA spirals for RC bridge piers and emergency repair technique for severely damaged piers. First three 1/3-scale RC piers were retrofitted with GFRP jackets, SMA spiral, and SMA spiral plus GFRP jackets, respectively, while one pier remained as-built. Then, the piers were tested under quasi-static cyclic lateral load. The results showed that the piers with the SMA spirals were able to sustain larger force and drift, and dissipate more hysteretic energy compared to those of the as-built pier and the GFRP retrofitted pier. The levels of damage which the tested piers sustained clearly demonstrated the superiority of the SMA spirals to the GFRP jackets in controlling the damage in the piers. Second, two piers (P1 and P2) that were severely damaged in a previous testing were repaired using the new confinement technique, and retested under quasi-static cyclic lateral load. The repair process of each pier was conducted in less than 15 hours and the piers were tested in less than 24 hours. Test results revealed that the lateral strengths and the initial stiffness of both repaired piers were fully restored or even enhanced. It is important to note that the recovered properties of the repaired piers are mainly attributed to the ability of the SMA spirals to apply and maintain active confining pressure on the damaged region of the piers, which increased the strength of the already damaged concrete and delayed its damage by increasing its ultimate strain. This paper showed that the proposed repair technique is effective and could be implemented successfully in a short time and thus could be used in emergency situations to maintain or restore the functionality of damaged lifeline structures. Finally, based on the testing results of the SMA pier, a fiber section based model of actively confined pier was developed and validated. The constitutive behavior of actively confined concrete was well implemented into the model while taking into account of the recovery stress and prestrain losses of the SMA spirals. The numerical results showed that the developed model is capable of capturing the hysteretic force and displacement relationship of the experimental pier within acceptable accuracy.

AKCNOWLEDGEMENT

The authors acknowledge the support for this study provided by the National Cooperative Highway Research Program through its Innovations Deserving Exploratory Analysis program (NCHRP-IDEA) under project no. 135, and by the National Science Foundation through its Faculty Early Career Development (CAREER) program under Award No. 1055640.

REFERENCES

Chai,Y.H., Priestley, M.J.N., and Seible, F. (1991). Seismic retrofit of circular bridge piers for enhanced flexural performance. **ACI Strut. J.:88(5)**, 572-584.

Lorenzis, L.D. and Tepfers, R. (2003). Comparative Study of Models on Confinement of Concrete Cylinders with Fiber-Reinforced Polymer Composites. **J. Composite for Construction. ASCE; 7(3)**, 219-37.

Mander, J.B., Priestley, M.J.N., and Park, R. (1988). Theoretical stress-strain model for confined concrete. **Journal of Structural Engineering (ASCE):114(8)**,1804–1826.

Mazzoni, S., McKenna, F., Scott, M.H., and Fenves, G.L. et al. (2009). OpenSees Command Language Manual. Open System for Earthquake Engineering Simulations.

Menegotto, M., and Pinto, P.E. (1973). Method of analysis of cyclically loaded RC plane frames including changes in geometry and non-elastic behavior of elements under normal force and bending. **Preliminary Report IABSE 13**, 15–22.

Priestley, M.J.N., Seible, F., Xiao, Y. and Verma, R. (1994). Steel jacket retrofitting of reinforced concrete bridge piers for enhanced shear strength-Part1: Theoretical considerations and test design. **ACI Struct. J.: 91(4)**, 394-405.

Schickert, G. and Winkler, H. (1977). Results of tests concerning strength and strain of concrete subjected to multiaxial compressive stresses. *Deutscher Ausschuss fur Stahlbeton,* Heft 277, Berlin, West Germany.

Shin, M, and Andrawes, B. (2010). Experimental investigation of actively confined concrete using shape memory alloys. **Engineering Structures:32(3)**, 656-664.

Richart, F.A., Brandtzaeg, A. and Brow, R. L. (1928). A study of the failure of concrete under combined compressive stress. *Bulletin 185, University of Illinois Engineering Experiment Station*, Urbana IL, 104.

Task Group 7.4. (2007). Seismic bridge design and retrofit—structural solutions. *fib Bulletin No.39,* International Federation for Structural Concrete, Lausanne, Switzerland.